X-Ray Diffraction and Dielectric Spectroscopy of Poly(ethylene terephthalate) and PET/Carbon Nanotube Nanocomposites

An honors thesis for the Departments of Physics and Astronomy

Bret Stenger

Tufts University, 2009

Table of Contents

Figures

Abstract

The crystallization of poly(ethylene terephthalate) (PET) and a nanocomposite of PET with multi-walled carbon nanotubes (MWCNTs) were studied by wide and small angle X-ray diffraction and dielectric relaxation spectroscopy. The purpose was to differentiate between a heterogeneous and homogeneous stack model to describe the lamellar organization in PET and to determine the effect of carbon nanotubes on the crystal growth in PET. The nanocomposites contained 2% MWCNT by weight, and were prepared by solution mixing, and then compression molding into film. Dielectric measurements were made at frequencies from 100 Hz to 1 MHz, in parallel plate geometry. Measurements of the samples during cold crystallization (100-120°C) were used to investigate the relationship between the growth of crystals and the restriction of the molecular mobility of the amorphous phase. Results indicate that a heterogeneous distribution of amorphous regions exists, implying both interlamellar and interfibrillar/interspherulitic placement of the amorphous chains. Addition of carbon nanotubes to the PET increased the rate of cold crystallization, but did not affect the glass transition relaxation process.

Introduction

Poly(ethylene terephthalate) (PET) is a thermoplastic polymer in the polyester family. It is composed of a chain of $C_{10}H_8O_4$ monomer units. PET has a melting temperature of 260°C and a glass transition temperature of 75°C. Common uses of PET include the production of synthetic fibers and soda bottles [1].

There are currently two different models describing the crystal structure of semi-crystalline polymers. Polymer crystals grow outward from a point, forming spherical crystalline aggregates called spherulites. The aggregates are formed from radially-grown ribbon crystals, called lamellae. Between the lamellae there are amorphous, or non-crystalline, regions.

At the interface between the crystalline (C) and mobile amorphous (MA) phases, there is a rigid amorphous fraction (RAF). The length of PET molecules allows sections of a single molecule to be in both the amorphous and crystalline phases. As a result, there exists a region where the material is in the amorphous phase, but many of the molecules are confined by being in proximity to a crystalline region. This restricts the ability of the molecules in the RAF to freely move [2].

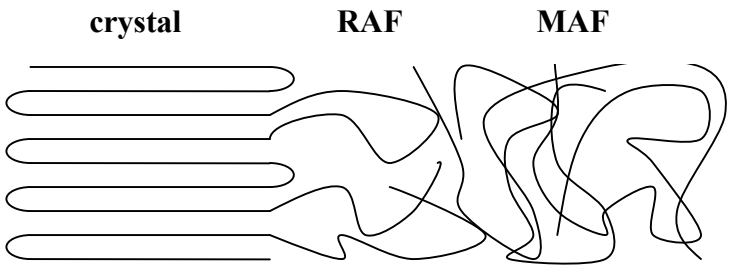

Figure 1: RAF at the boundary between the crystalline and mobile amorphous phases.

In the Heterogeneous Stack Model (HET) (Figure 2, right side), there are large amorphous regions interspersed between crystalline regions. Between lamella in the crystalline regions there is only rigid amorphous fraction. The molecular mobility of the rigid amorphous phase is restricted during the initial crystallization of the material [3].

In the Homogeneous Stack Model (HSM) (Figure 2, left side), the lamellae are distributed evenly around the spherulite. There is an amorphous region between lamella. The RAF is a boundary layer. Crystallization does not restrict the mobility of the amorphous regions before spherulite impingement. After spherulite impingement has occurred, secondary crystallization develops in the amorphous regions, restricting molecular mobility [4].

Figure 2 is a simplified depiction of the HET and HSM showing the arrangement of the crystal, mobile amorphous, and rigid amorphous regions. In reality, the lamellae are not in wedge shapes as depicted, but are sheets that branch as they grow from the center of the spherulite. Also, the distance between lamellae does not increase with distance from the center of the spherulite, but instead is constant.

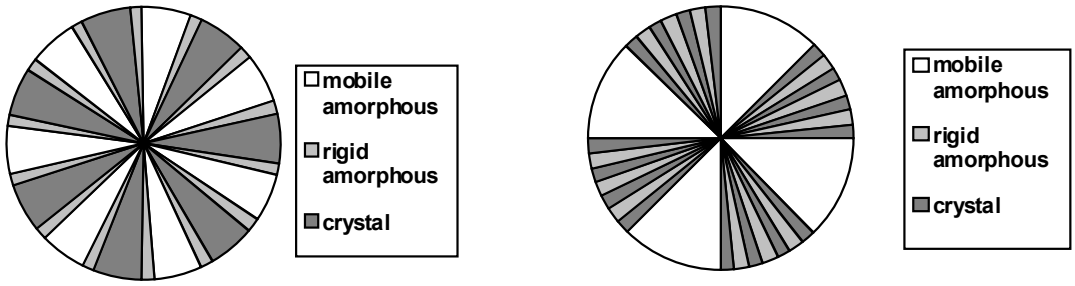

Figure 2: The Homogeneous Stack Model (left) and Heterogeneous Stack Model (right)

A carbon nanotube is a thin cylinder of carbon with a diameter on the order of nanometers and a length on the order of microns. It is composed of a hexagonal lattice of carbon atoms, similar to a graphite sheet, rolled into a tube [5]. The first observation of carbon nanotubes was made by Sumio Iijima in 1991 [6]. Since their discovery carbon nanotubes have been studied extensively due to their unique properties, including high strength, thermal conductivity, and interesting electrical properties [7].

Theoretical Analysis

1. Dielectric Spectroscopy

When an alternating electric field is applied to a material composed of molecular dipoles, dielectric relaxation occurs. The electric dipoles of the molecules in the material experience a torque causing them to align themselves with the field. As the field oscillates, the dipoles will alternate their direction to follow the field. The ability of the dipoles to align themselves with the field relates to the molecular mobility of the material.

This phenomenon can be described by the complex dielectric permittivity of the material, ε*. ε* is defined as [8]

$$\varepsilon^* = \varepsilon' - i\varepsilon'' \quad (1)$$

The real component of the complex dielectric permittivity, ε', is the relative dielectric constant. This is a measure of the energy stored by the material. The imaginary component of the complex dielectric permittivity, ε", is the dielectric loss factor. This represents the dissipation of energy during relaxation.

Dielectric relaxation is dependent on the frequency of the oscillation of the electric field. Higher frequencies will cause the diploes to realign themselves more rapidly. This results in a dissipation of energy and an increase in ε". At high frequencies, due to the inertia of the dipoles, they are unable to align themselves quickly enough to keep up with the oscillations of the electric field. A lag between the orientation of the dipoles and the electric field develops. Less energy is dissipated and ε" decreases. As a result, dielectric relaxation will appear as a peak in ε" at the relaxation frequency, the frequency at which the most energy is dissipated with oscillations of the electric field.

At frequencies above the relaxation frequency, the dipoles are no longer able to completely align themselves with the electric field. Therefore, less energy can be stored in the material. As a result, ε' is lower at frequencies above the relaxation frequency. The difference between ε' at frequencies higher and lower than the relaxation frequency is a measure of the number and strength of the dipoles involved in the relaxation.

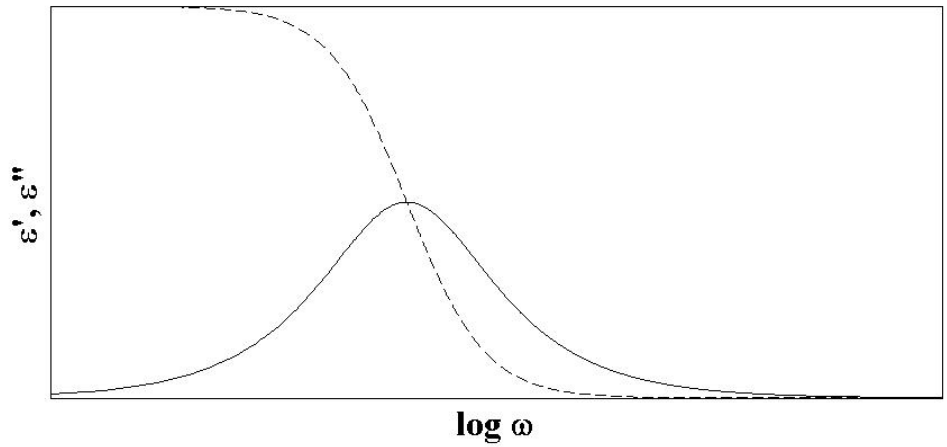

Figure 3: Typical plot of ε'' (undotted line) and ε' (dotted line) vs. angular frequency

ε’ and ε” can be calculated from the capacitance, C, and the dissipation factor, D. For measurements made in parallel with parallel plate electrodes, ε’ is given by [8]

$$\varepsilon' = \frac{C}{C_0} \tag{2}$$

C_o, the empty cell capacitance, depends on the geometry of the electrodes and is given by

$$C_0 = \frac{A\varepsilon_0}{d} \tag{3}$$

where A is the area of the electrodes, d is the separation between the electrodes, and ε_0 is the permittivity of a vacuum, $\varepsilon_0 = 8.854 \times 10^{-12}$ F/m.

D relates to ε’ and ε” by the equation

$$D = \frac{\varepsilon''}{\varepsilon'} \tag{4}$$

Therefore,

$$\varepsilon'' = \frac{C}{C_0} D \tag{5}$$

2. X-Ray Diffraction

The periodic spacing within a material can be determined through x-ray diffraction. When passing through a lattice, X-ray radiation will scatter at an angle dependent on the periodic spacing of the lattice according to Bragg's Law [9],

$$2d\sin(\theta) = n\lambda \tag{6}$$

where d is the periodic spacing, λ is the wavelength of the incident X-ray radiation, and n is the order of the scattering. θ is the angle of the incident and scattered beams from the plane of scattering, so the angle of scattering between the incident and scattered X-rays is 2θ.

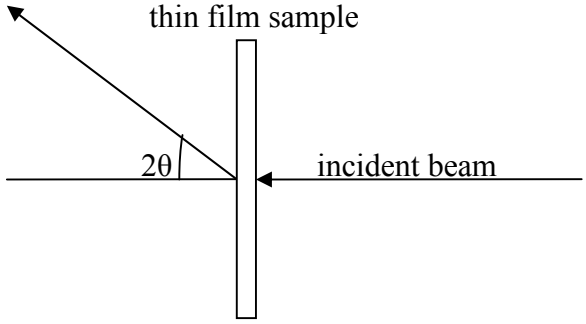

Figure 4: Geometry of scattering of X-rays from a thin film at angle 2θ.

Wide-angle X-ray scattering (WAXS) refers to X-ray scattering at scattering angles, 2θ, of greater than 5°. This corresponds to separation distances on the order of angstroms. This is the length scale of the atomic spacing in the crystals of polymers.

In small-angle X-ray scattering (SAXS), lower angles of scattering are used to study larger-scale structure in a material. Angles of scattering below 5° result from distances on the order of nanometers in the material. The lamellar thickness and spacing in PET are on this order of length. SAXS intensities are typically shown as a function of the scattering vector, q, defined as:

$$q = \frac{4\pi}{\lambda} \sin\theta \tag{7}$$

where λ is the wavelength of the incident X-rays, and 2θ is the angle of scattering. The scattering vector, q, is related to the periodic spacing in the material, d, by

$$q = \frac{2\pi}{d} \tag{8}$$

In order to clearly show the peaks from the lamellar structure of a material, it is necessary to perform a Lorentz correction on the SAXS intensity. The Lorentz-corrected intensity is given by

$$I_{corrected} = Iq^2 \tag{9}$$

where I is the uncorrected intensity and q is the scattering vector. The Lorentz correction sets the intensity to zero at a scattering angle of zero, preventing the plot of intensity vs. scattering vector, q, from being dominated by low angle scattering [8].

Experimental Apparatus

1. Dielectric Spectroscopy

Dielectric measurements were made with two different apparatuses. In the first apparatus, shown in Figure 5, the thin film sample was placed between two 100 μm thick aluminum disks. The sample and aluminum disks were placed between two circular brass electrodes, shown in Figure 6. There was a hole through the center of each brass electrode so that X-rays could pass through without being absorbed by the electrode. The aluminum disks improved heat transfer and prevented the holes in the electrodes from creating an uneven heat distribution across the surface of the sample. Aluminum is highly

transparent to X-rays and has a thermal conductivity of 250 W/mK at room temperature compared to 109 W/mK for brass. A wire was inserted into a small hole in the edge of each electrode. The electrodes were pressed to pinch and secure the wires in the holes. As shown in Figure 5, each wire was connected to a pair of BNC cables. The BNC cables were connected to a Hewlett-Packard 4284A Precision LCR Meter. The cables from one wire (upper electrode) led to the high voltage and current ports of the LCR Meter and the cables from the second wire (lower electrode) led to the low voltage and current ports of the LCR Meter. The LCR meter was connected to a computer with an Agilent Technologies 82357B USB/GPIB Interface. The electrode sandwich was wrapped in Kapton tape to maintain contact between the electrodes and the sample while electrically insulating it from the heating plates. The sandwich was placed in a Mettler Toledo FP82HT Hot Stage.

The LCR meter was controlled by a graphical user interface (GUI) computer program written in Matlab^{TM} by Lei Yu [9]. The program, called Real-time Dielectric, could be set to measure up to 30 different frequencies, ranging from 20 Hz to 1 MHz. The frequencies were accurate to ± 0.1%. A single measurement could be made at each frequency, or alternatively measurements could be taken continuously over a set period of time. The program instructed the LCR meter to pass a current through the electrodes and sample at the specified frequencies. The LCR meter measured the capacitance, C, and the dissipation factor, D, of the sample. The real and imaginary components of the complex dielectric constant, ε' and ε", at each frequency were calculated from C and D and stored on the computer. The capacitance was measured with an accuracy of ± 0.5% and the dissipation factor was measured with an accuracy of ± 0.0005.

The temperature of the sample was controlled by the Mettler Toledo FP82HT Hot Stage. The temperature of the hot stage oven could range from room temperature to 375 °C with an accuracy of ± 0.8°C. The oven was heated by two heating plates, located above and below the sample.

The LCR meter was calibrated with open and short tests. In the short tests, a measurement was made with the two electrodes in contact. In the open tests, a measurement was made with the electrodes several inches apart, to simulate an infinite distance. The LCR meter could use these measurements to correct for any resistance introduced by the cables and wires between the LCR meter and the electrodes.

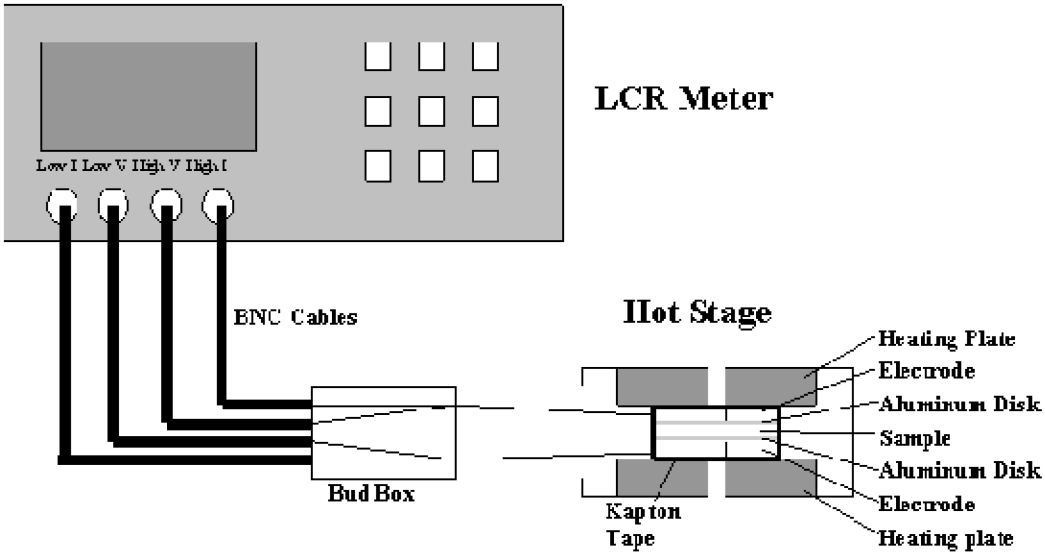

Figure 5: Dielectric apparatus

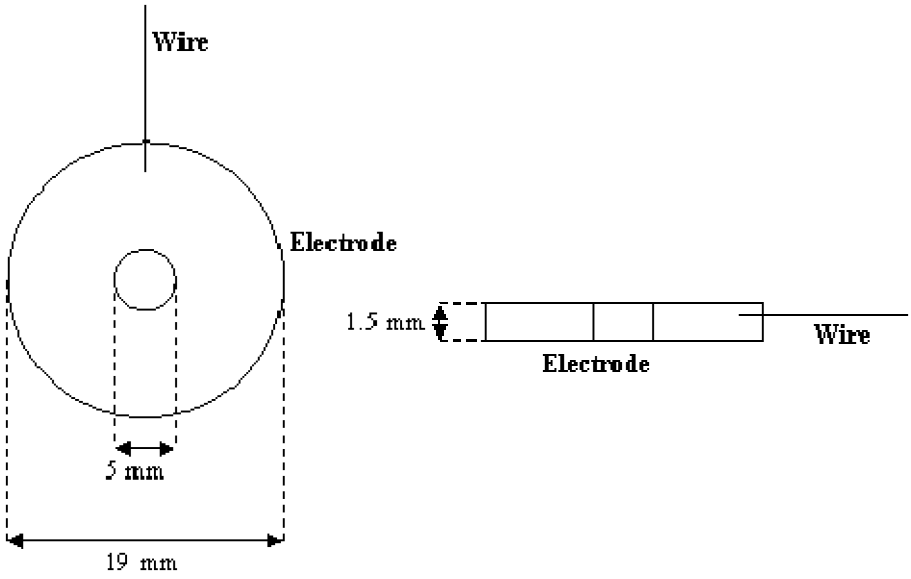

Figure 6: Brass electrodes showing center hole and wire placement in top view (left) and side view (right)

The second dielectric apparatus, shown in Figure 7, consisted of a TA Instruments ARES Rheometer with the ARES Dielectric Thermal Analyzer accessory and a Hewlett-Packard 4284A Precision LCR Meter. The thin film sample was placed between two circular parallel plate electrodes inside the air convection oven of the ARES, shown in Fgure 4. The ARES and the LCR meter were controlled by TA Orchestrator software on a computer. The temperature of the oven and the size of the gap between the electrodes were set with the software. The temperature could be set within the range of -150°C to 300°C with a stability of ± 0.1°C. Liquid nitrogen was used to cool the oven below room temperature. Measurements could be taken in either the temperature step mode or the temperature ramp mode. In the temperature step mode, the temperature was held constant at set intervals over a range of temperature. At each interval, measurements were made at the specified frequencies. In temperature ramp mode, measurements were made continuously as the temperature was varied. In either mode, up to ten different

frequencies could be measured at a time. The frequencies could be set between 20 Hz and 1 MHz with accuracy of 0.1%. The LCR meter measured the capacitance and the dissipation factor of the sample. The real and imaginary components of the complex dielectric constant, the capacitance, the dielectric loss, and the dielectric loss tangent could be displayed and stored on the computer. The capacitance was measured with an accuracy of ± 0.5% and the dissipation factor was measured with an accuracy of ± 0.0005.

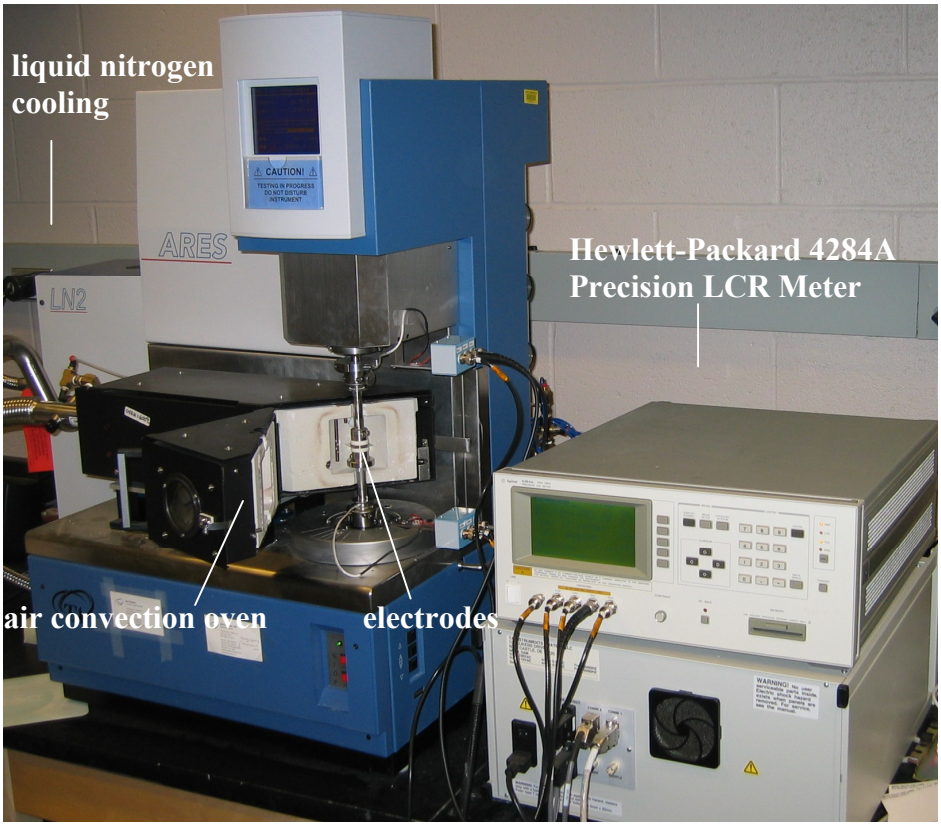

Figure 7: ARES Dielectric Apparatus

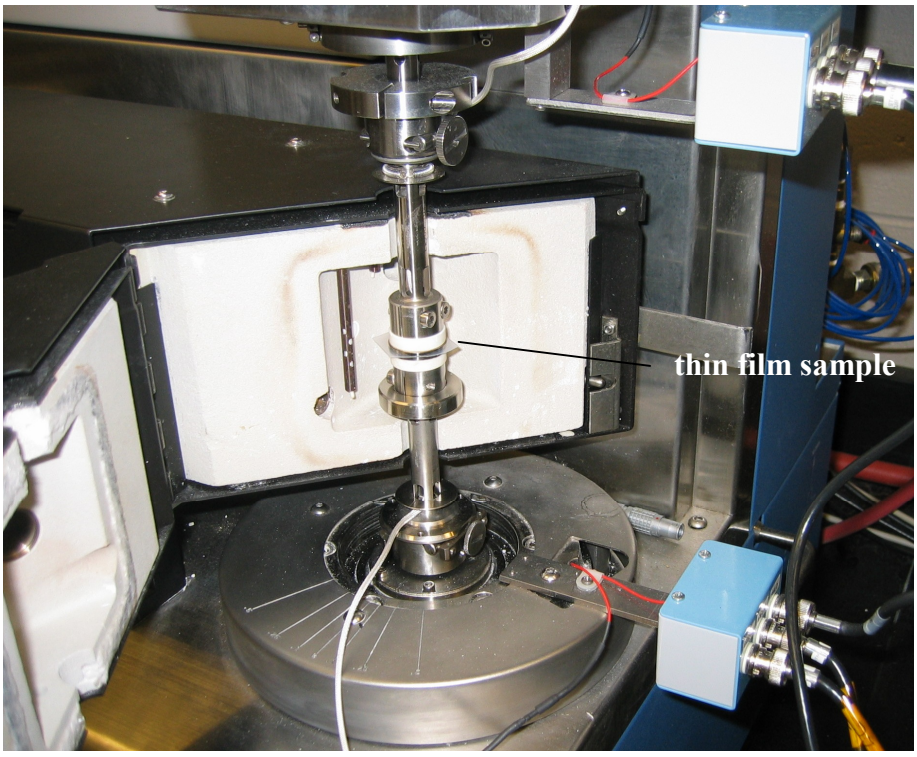

Figure 8: ARES air convection oven and electrodes

2. X-ray Diffraction

Real-time WAXS and SAXS measurements were made at the X27C Advanced Polymer Beamline at the National Synchrotron Light Source at Brookhaven National Laboratory. The incident X-ray beam had a wavelength of 0.1371 nm.

During X-ray diffraction without simultaneous dielectric measurements, the sample was wrapped in Kapton tape and placed inside a Mettler Toledo FP82HT Hot Stage, covering the aperture. With simultaneous dielectric measurements, the sample was placed in the dielectric cell shown in Figure 5. The hot stage was then placed in a holder and aligned so that the X-ray beam could pass though the aperture of the hot stage.

The X-rays were detected by two 1-D position sensitive European Molecular Biology Laboratory detectors, one placed close to the sample for WAXS measurements

and one placed further from the sample for SAXS measurements. Aluminum oxide (Al_2O_3) was used as the standard of calibration for the WAXS detector. Silver Behenate (AgBe) was used as the standard of calibration for the SAXS detector. Aluminum sheets were placed in front of the SAXS detector to adjust the intensity of the X-rays to prevent damage to the detector.

X-ray diffraction measurements were made continuously during isothermal crystallization with consecutive 60 second scans.

The background of the X-ray scattering was collected for each measurement. The WAXS and SAXS patterns of Kapton tape and of Kapton tape with aluminum were collected for measurements of samples only wrapped in Kapton tape and samples placed in the dielectric cell, respectively. The background measurements were made at the same temperature as the original measurements. The background was subtracted from each measured diffraction pattern with a program written in Matlab™ by Peggy Cebe [10].

Room temperature WAXS measurements were made with a Bruker AXS D8 Discover X-ray Diffractometer (Figure 9). A thin film sample was placed in the sample holder. The incident X-ray beam had a wavelength of 0.154 nm. The scattered X-rays were detected by a 2D HI-STAR Area Detector. The data are integrated over a sector to produce a 1-dimensional WAXS pattern from the 2-dimentional data collected by the detector.

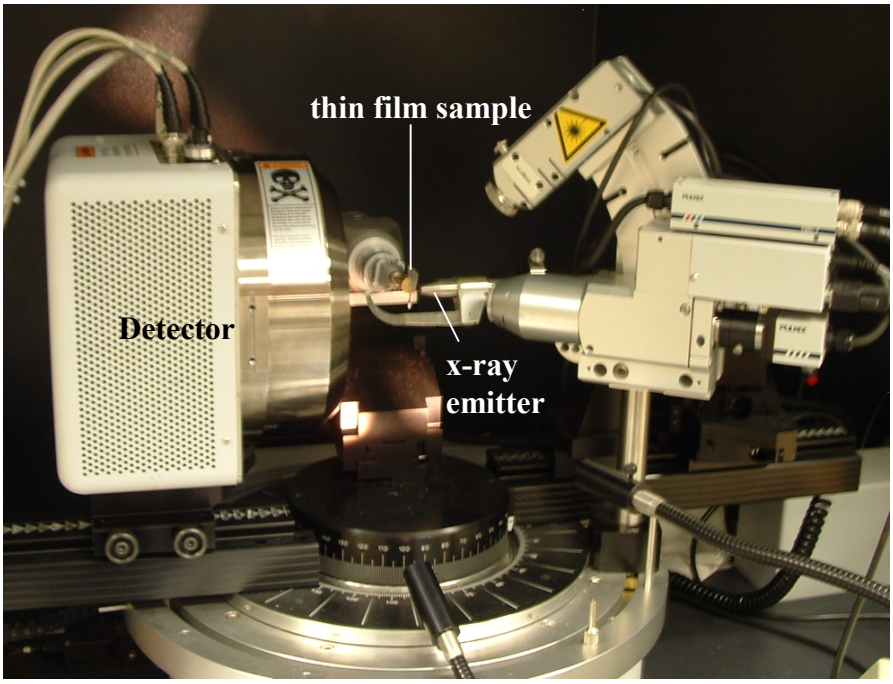

Figure 9: Bruker AXS D8 Discover X-ray Diffractometer

Results

1. Wide-angle X-ray Scattering After Isothermal Crystallization at 100°C

WAXS intensity vs. scattering angle is shown in Figure 10 for PET held isothermally at 100°C for different times. Measurements were made at room temperature. The WAXS pattern for the amorphous sample of PET (Fig. 10a) has a broad amorphous halo. In the sample with 15 minutes of crystallization (Fig. 10b) there is no significant change from the amorphous sample, indicating that it is still in the amorphous phase. With 30 minutes of crystallization, peaks appear at scattering angles, 2θ, of 16.9°, 18.2°, and 25.7°. These peaks have miller indices of (100), (-110), and (010) and correspond to atomic plane separation distances of 0.47 nm, 0.43 nm, and 0.31 nm, respectively. The WAXS pattern of the sample with 60 minutes of crystallization has no significant change

from the sample with 30 minutes of crystallization. This indicates the majority of the crystal growth occurs between 15 minutes and 30 minutes of isothermal crystallization at 100°C.

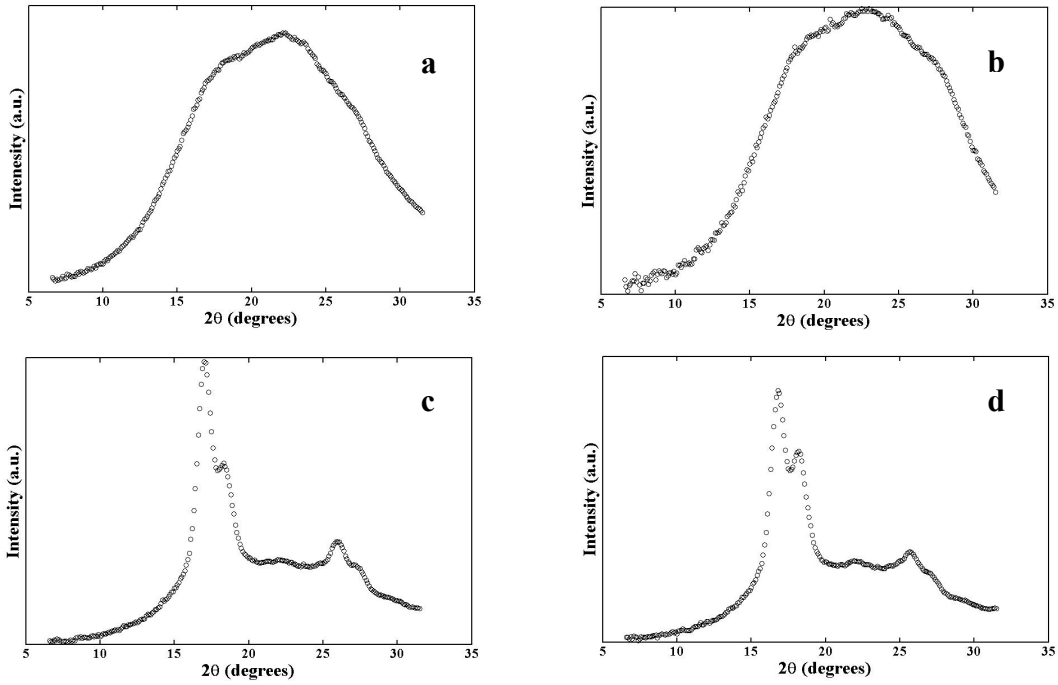

Figure 10: WAXS intensity vs. scattering angle, 2θ, of PET at room temperature after isothermal crystallization at 100°C for 0 (a), 15 (b), 30 (c), and 60 (d) minutes

2. Dielectric Spectroscopy After Isothermal Crystallization at 100°C

Figure 11 shows the dissipation factor vs. frequency for PET after isothermal holding at 100°C. The same samples used for X-ray in Figure 10 were reheated to 95°C for dielectric experiments. Measurements were made at 95°C so that the relaxation peak would be located in the measured frequency range. In the amorphous sample of PET there is a relaxation peak at 30 kHz. With 15 minutes of crystallization (Fig. 10b), there is a drop in the relaxation peak, indicating a restriction of the molecular mobility of the sample due to crystallization. This is not consistent with the fully amorphous WAXS

pattern shown in Figure 10b but can be explained by crystallization of the sample while holding at 95°C during the dielectric measurement. In the sample with 30 minutes of crystallization (Fig. 11c), the relaxation peak drops further, and a second relation peak appears at 200 Hz. There is no significant change in the relaxation peaks between the 30 minute and 60 minute crystallization samples (Fig. 11d), indicating that little further crystallization occurs after the first 30 minutes.

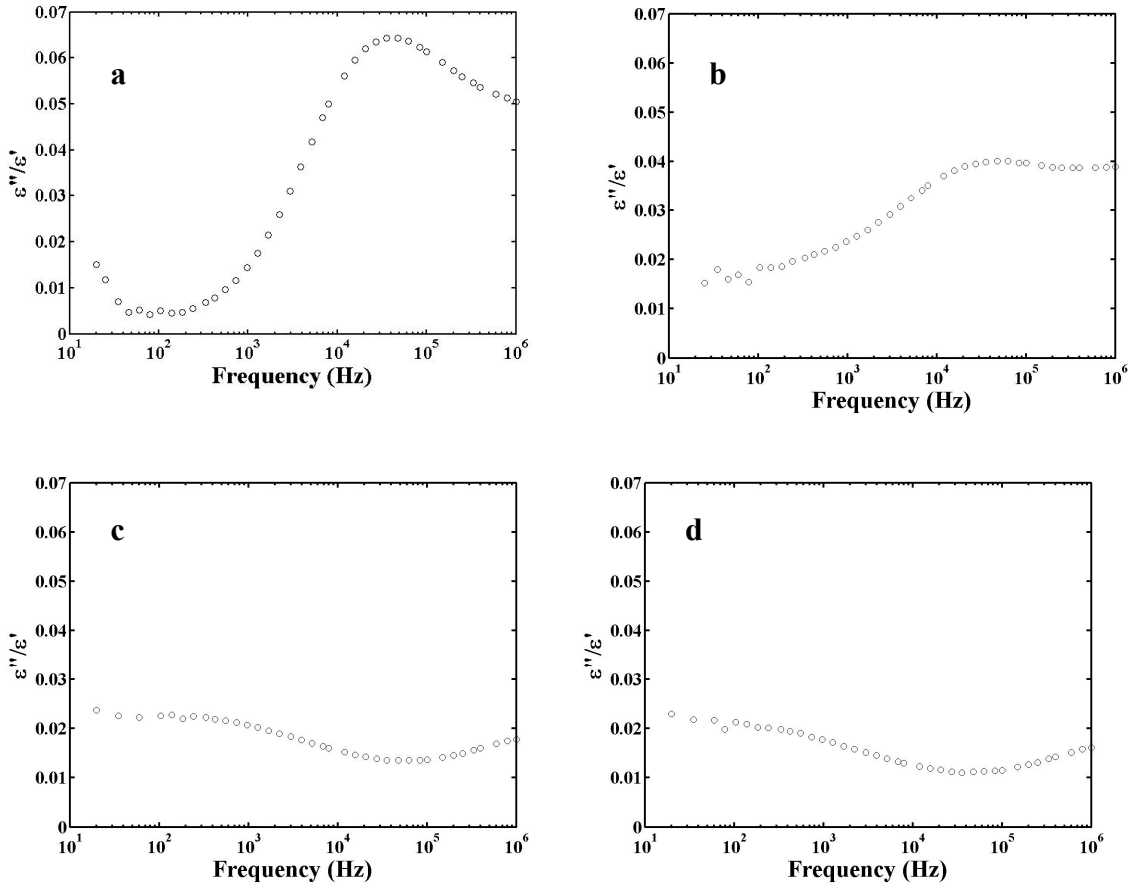

Figure 11: Dissipation factor, ε''/ε', vs. frequency of PET at 95°C after isothermal crystallization at 100°C for 0 (a), 15 (b), 30 (c) and 60 (d) minutes.

3. Real-time Wide-angle X-ray Scattering During Isothermal Crystallization at 110°C and 120°C

Figure 12a shows a broad peak in the WAXS pattern of the PET sample at the start of crystallization confirming that the sample is in a mostly amorphous state. A small peak at a scattering angle, 2θ, of 23° shows that crystallization has begun during the first minute that the sample is held at 110°C. As the sample is crystallized at 110°C, there is a gradual decrease in the amorphous halo and a growth of peaks at scattering angles, 2θ, of 23° and 16°. Scattering at these angles corresponds to periodic separation distances in the material of 0.34 nm and 0.49 nm. There is no significant change in the WAXS pattern after 15 minutes, indicating that the sample has finished crystallizing.

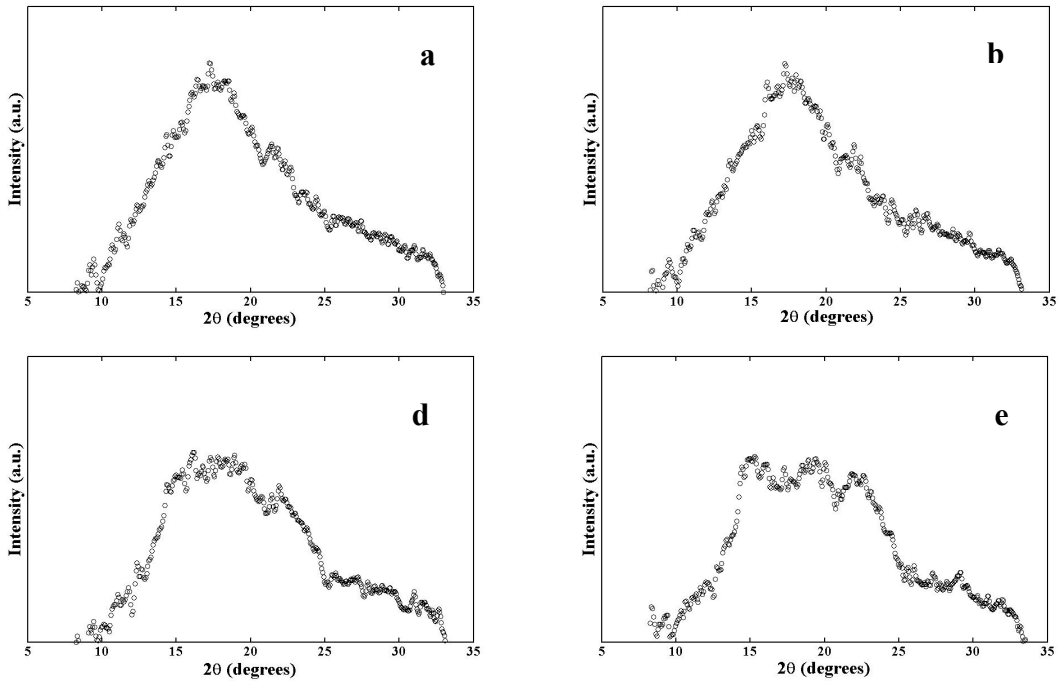

Figure 12: Real-time WAXS intensity vs. scattering angle, 2θ, of PET during isothermal crystallization at 110°C for 0 (a), 3 (b), 10 (c), and 15 (d) minutes

As expected, the crystallization process is more rapid during crystallization at 120°C, as shown in Figure 13. At 3 minutes of crystallization (Fig. 13b), crystallization peaks have developed. The peaks develop at the same angles of scattering as during crystallization at 110°. After 3 minutes, the rate of growth of the scattering peaks decreases indicating a slowing in the crystallization of the sample. There is no significant change in the WAXS pattern after 10 minutes, showing that the sample has finished crystallizing.

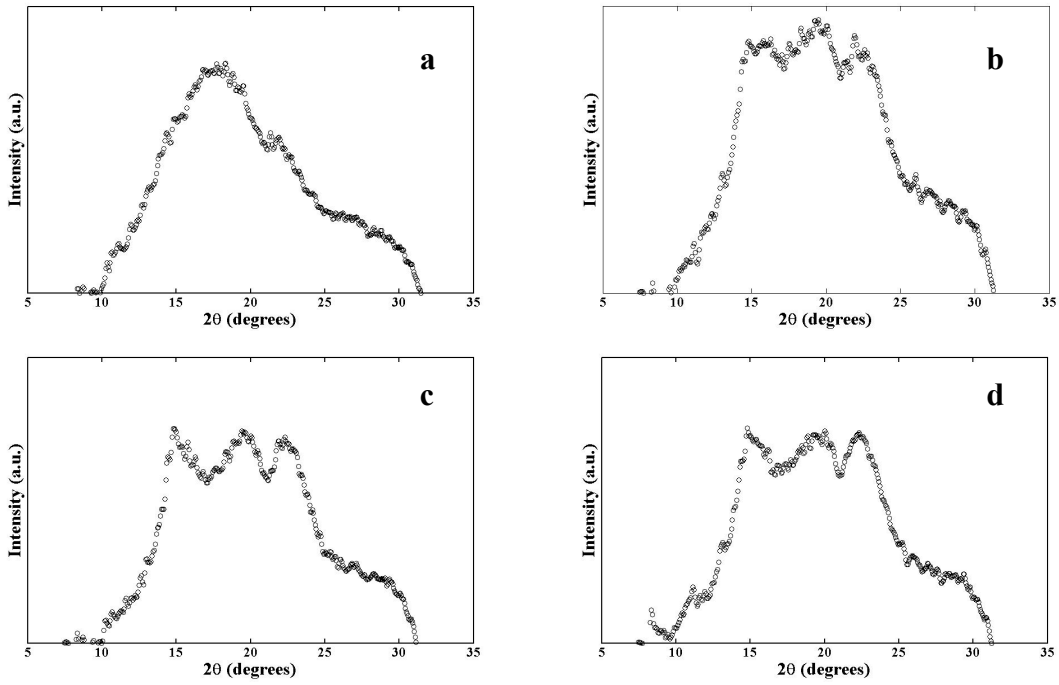

Figure 13: Real-time WAXS intensity vs. scattering angle, 2θ, of PET during isothermal crystallization at 120°C for 0 (a), 3 (b), 10 (c), and 15 (d) minutes

The rate of crystallization is greater for the PET/CNT nanocomposite than for neat PET, as shown in Figure 14. At 3 minutes of crystallization at 110° (Fig. 14b), crystallization peaks have begun to develop at scattering angles, 2θ, of 23° and 16° as

seen in the crystallization of pure PET. After 6 minutes of crystallization, there is no significant change in the WAXS pattern.

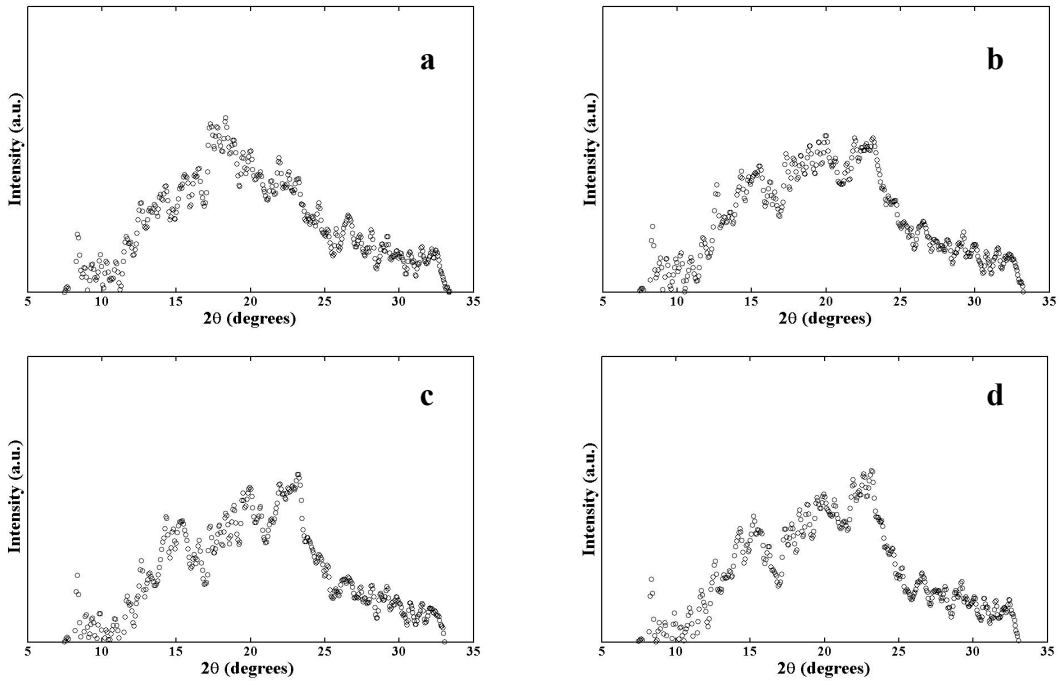

Figure 14: Real-time WAXS intensity vs. scattering angle, 2θ, of PET/CNT nanocomposite during isothermal crystallization at 110°C for 0 (a), 3 (b), 10 (c), and 15 (d) minutes

During crystallization of the PET/CNT nanocomposite at 120°C, shown in Figure 15, the peak at a scattering angle of 23° is visible during the first minute. At 3 minutes, peaks at 23° and 16° are well developed. After 3 minutes of crystallization, there is no significant change in the WAXS pattern.

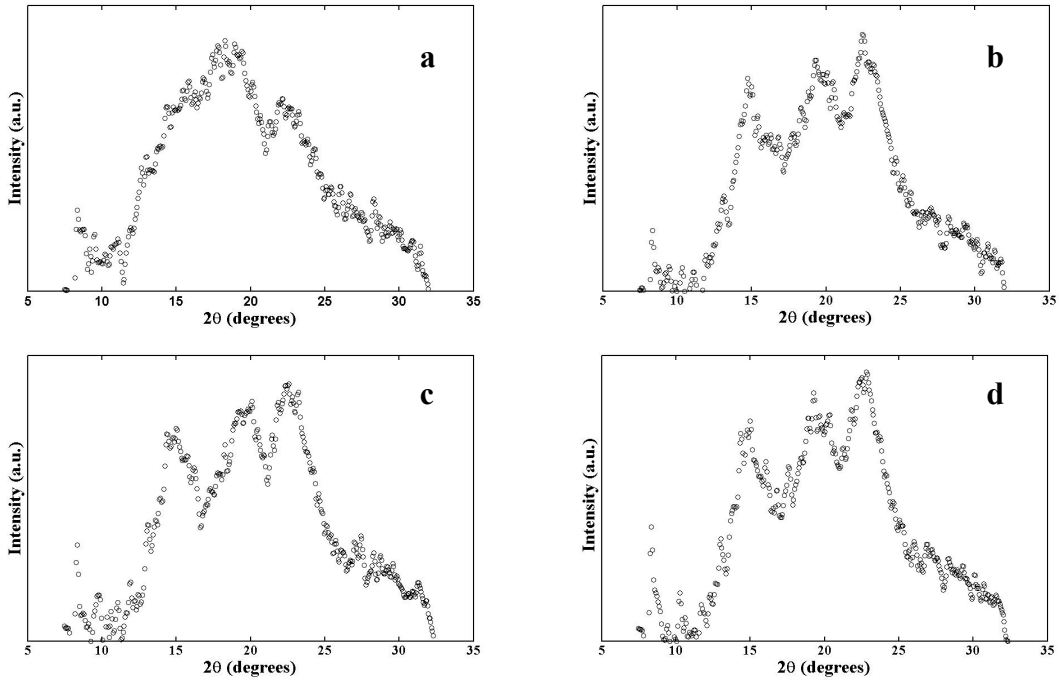

Figure 15: Real-time WAXS intensity vs. scattering angle, 2θ, of PET/CNT nanocomposite during isothermal crystallization at 120°C for 0 (a), 3 (b), 10 (c), and 15 (d) minutes

4. Real-time Small-angle X-ray Scattering During Isothermal Crystallization at 110°C and 120°C

A plot of the Lorentz corrected SAXS intensity $I(q)q^2$ vs. q, for PET during isothermal crystallization at 110°C is shown in Figure 16. After 7 minutes of crystallization a peak begins to develop at a q-value of 0.8 nm^{-1}. This corresponds to a separation distance of 7.9 nm. The peak continues to grow until 13 minutes of

crystallization. After 13 minutes, there is no significant change in the SAXS peak, indicating that crystallization has finished.

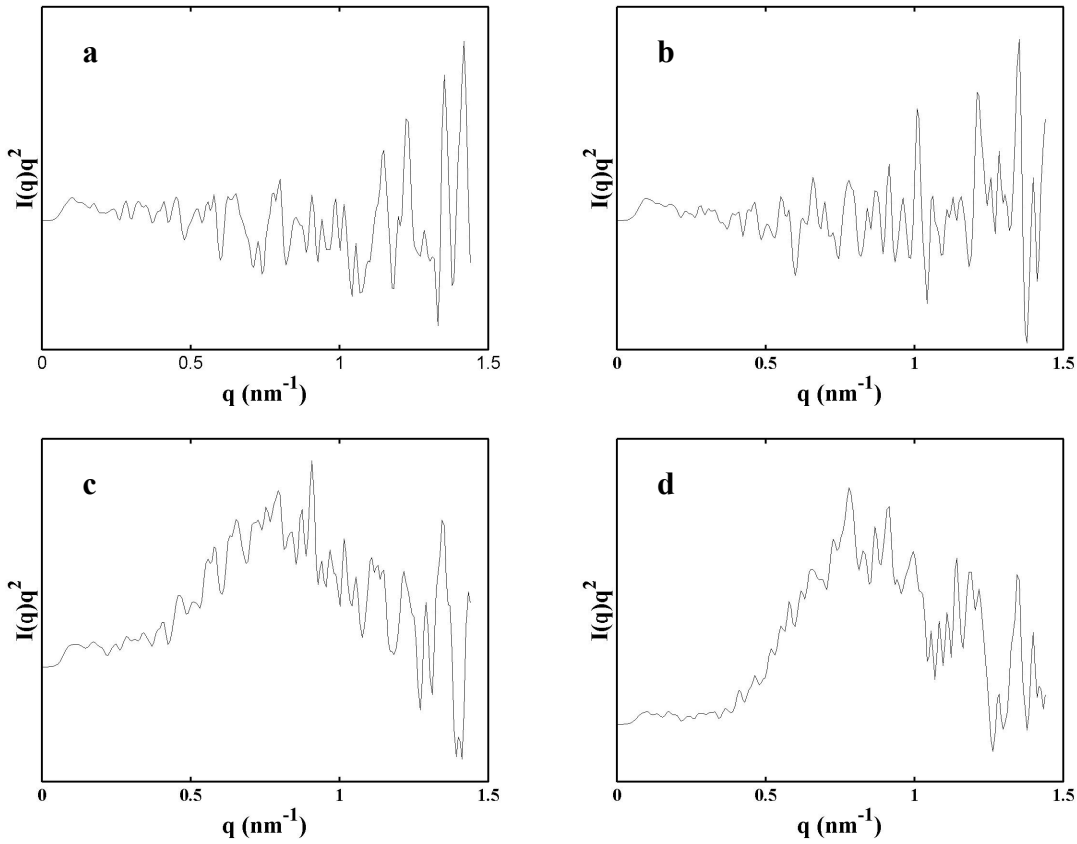

Figure 16: Lorentz-corrected, real-time SAXS intensity vs. scattering vector, q, of PET during isothermal crystallization at 110°C for 0 (a), 3 (b), 10 (c), and 15 (d) minutes

The crystallization process occurs more rapidly at 120°C, as shown in Figure 17. A SAXS peak develops after 2 minutes at approximately the same q-value as the peak during crystallization at 110°C. After 4 minutes there is no significant change in the SAXS peak.

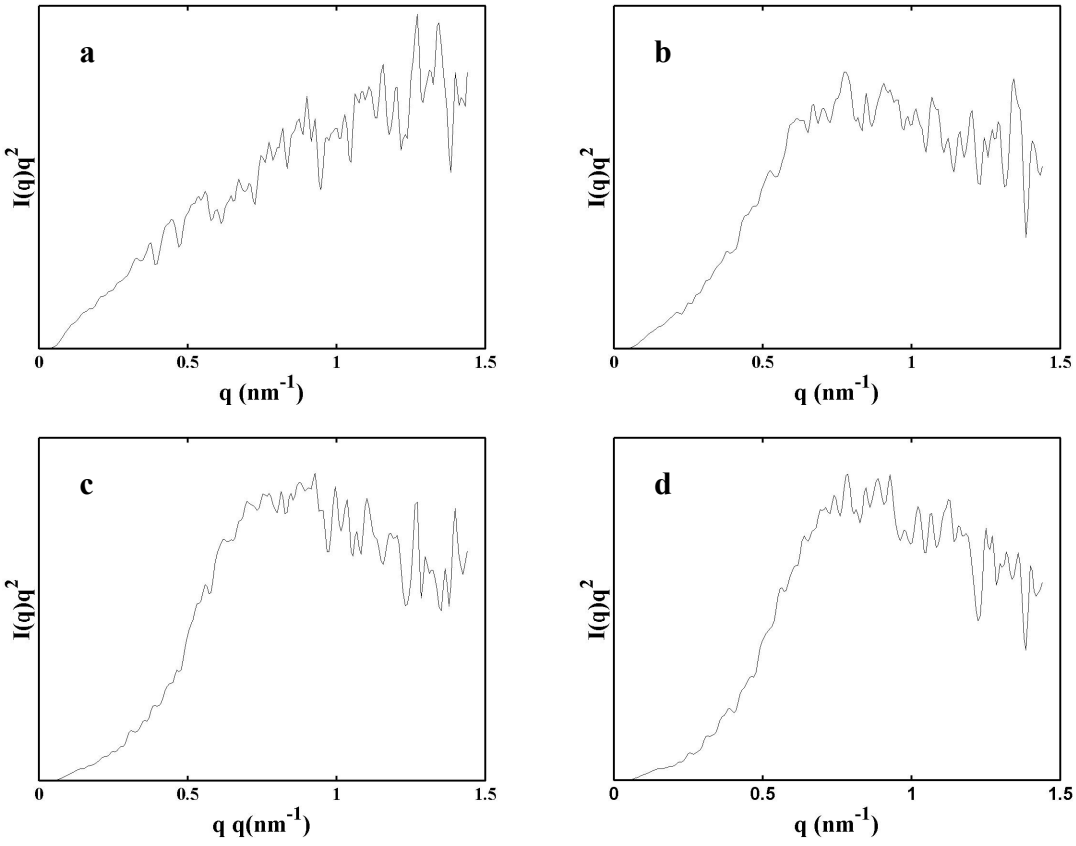

Figure 17: Lorenz-corrected, real-time SAXS intensity vs. scattering vector, q, of PET during isothermal crystallization at 120°C for 0 (a), 3 (b), 10 (c), and 15 (d) minutes

The initial SAXS pattern for the PET/CNT nanocomposite before crystallization at 100°C is shown in Figure 18a. A SAXS peak begins to develop at a q-vector of 0.8 nm^{-1}, the same location as the peak with neat PET, after 2 minute of crystallization. After 4 minutes there is no significant change in the SAXS peak. The peak in intensity at a q-vector of 0.15 nm^{-1} is an artifact caused by scattering of X-rays from the beam stop at the end of the beamline.

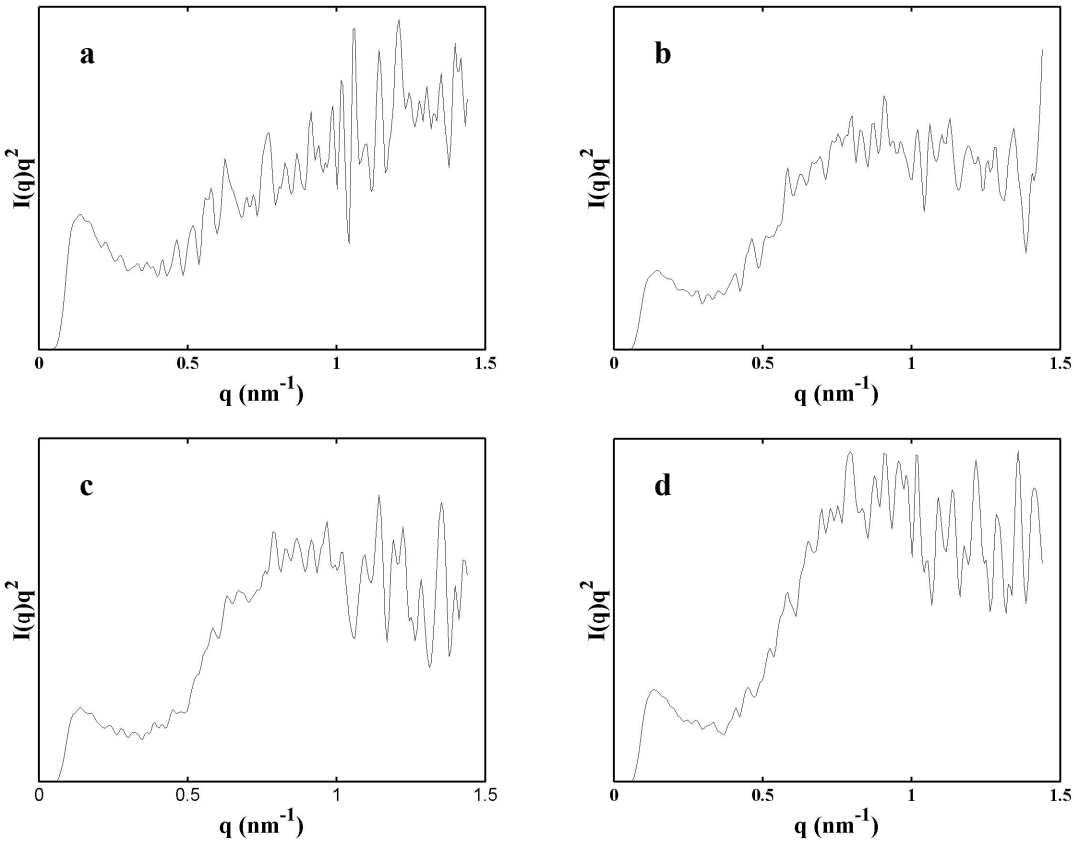

Figure 18: Lorentz-corrected, real-time SAXS intensity vs. scattering vector, q, of PET/CNT nanocomposite during isothermal crystallization at 110°C for 0 (a), 3 (b), 10 (c), and 15 (d) minutes

During crystallization of the PET/CNT nanocomposite at 120°C the SAXS peak first develops after 2 minutes of crystallization. After 3 minutes of crystallization there is no significant change in the SAXS peak.

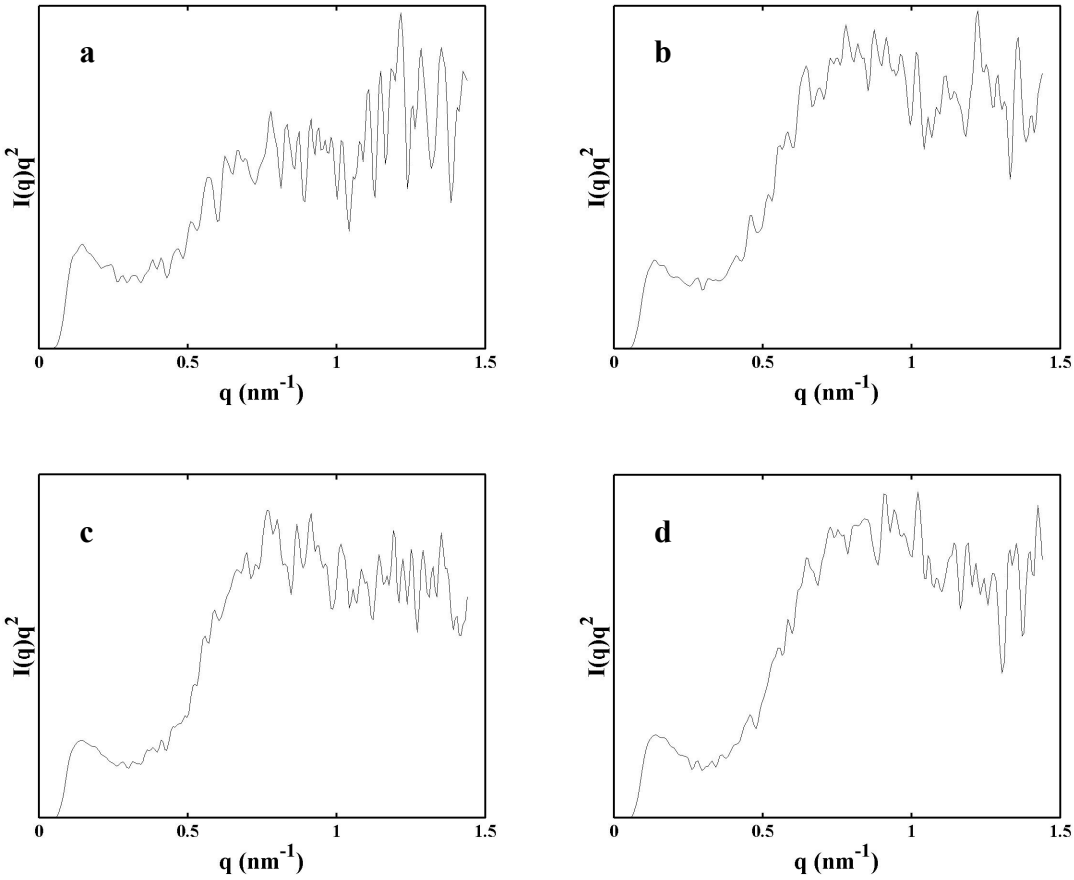

Figure 19: Lorentz-corrected, real-time SAXS intensity vs. scattering vector, q, of PET/CNT nanocomposite during isothermal crystallization at 120°C for 0 (a), 3 (b), 10 (c), and 15 (d) minutes

5. Real-time Dielectric Spectroscopy During Isothermal Crystallization at 110°C and 120°C

Figures 20 and 21 show the time development of the dissipation factor vs. frequency for PET crystallized at 110°C and 120°C, respectively. When the temperature is first raised to 110°C, the amorphous PET has a relaxation peak in the plot of ε"/ε' at frequency of 250 Hz. As the sample is held at 110°C, the relaxation peak increases and shifts to higher frequencies. This shift in peak position can be attributed to a lag between the temperature of the oven and the temperature of the sample during the initial heating. At 10 minutes (Fig. 20b), the relation peak is located at 10 kHz. After 17 minutes, the relaxation peak intensity drops and the peak broadens. The drop in the peak intensity indicates a restriction of molecular mobility from crystallization. After 30 minutes (Fig. 20e), the peak shifts to lower frequencies. The shift of the peak can be attributed to the development of a secondary crystallization process, occurring after spherulite impingement.

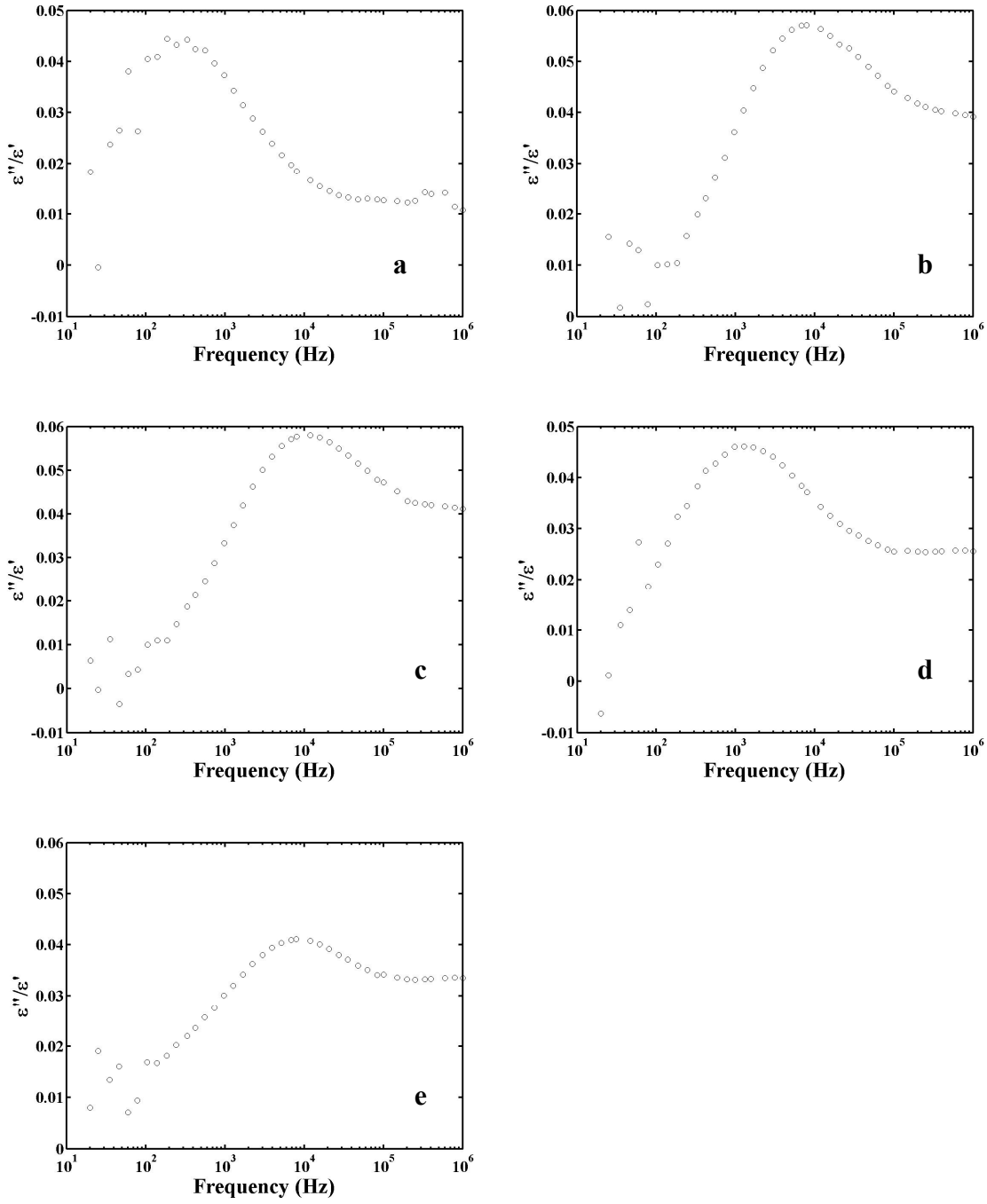

Figure 20: Dissipation factor, ε''/ε' vs. frequency of PET during isothermal crystallization at 110°C for 0 (a), 10 (b), 15 (c), 20 (d), and 30 (e) minutes

When the temperature is first raised to 120°C (Fig. 21a), the amorphous PET in the plot of ε"/ε' as a function of frequency has a peak at 560 Hz. During the first 12 minutes at 120°C, the peak increases and shifts to higher frequencies. At 10 minutes (Fig. 21b) the peak is located at a frequency of 30 kHz. After 19 minutes, the peak intensity begins to drop. After 26 minutes, the peak position begins to shift to lower frequencies.

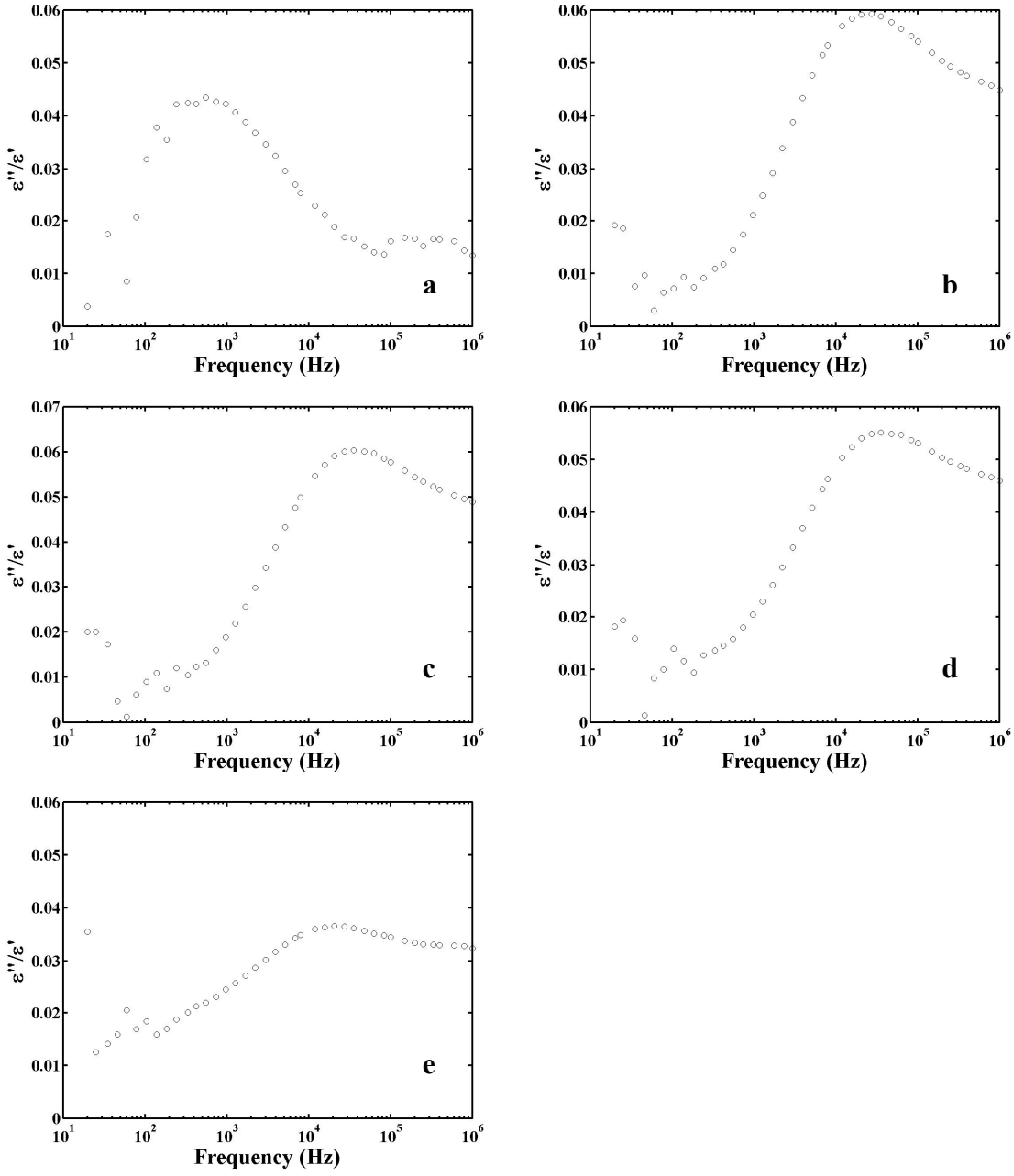

Figure 21: Dissipation factor, ε''/ε' vs. frequency of PET during isothermal crystallization at 120°C for 0 (a), 10 (b), 15 (c), 20 (d), and 30 (e) minutes

When the temperature is first raised to 120°C (Fig. 22a), the PET/CNT nanocomposite has a relaxation peak at a frequency of 10 kHz. During the first 7 minutes, the peak increases and shifts to higher frequencies. At 7 minutes the peak is located at

150 kHz. After 7 minutes, the peak intensity begins to drop. After 12 minutes the peak position begins to shift to lower frequencies.

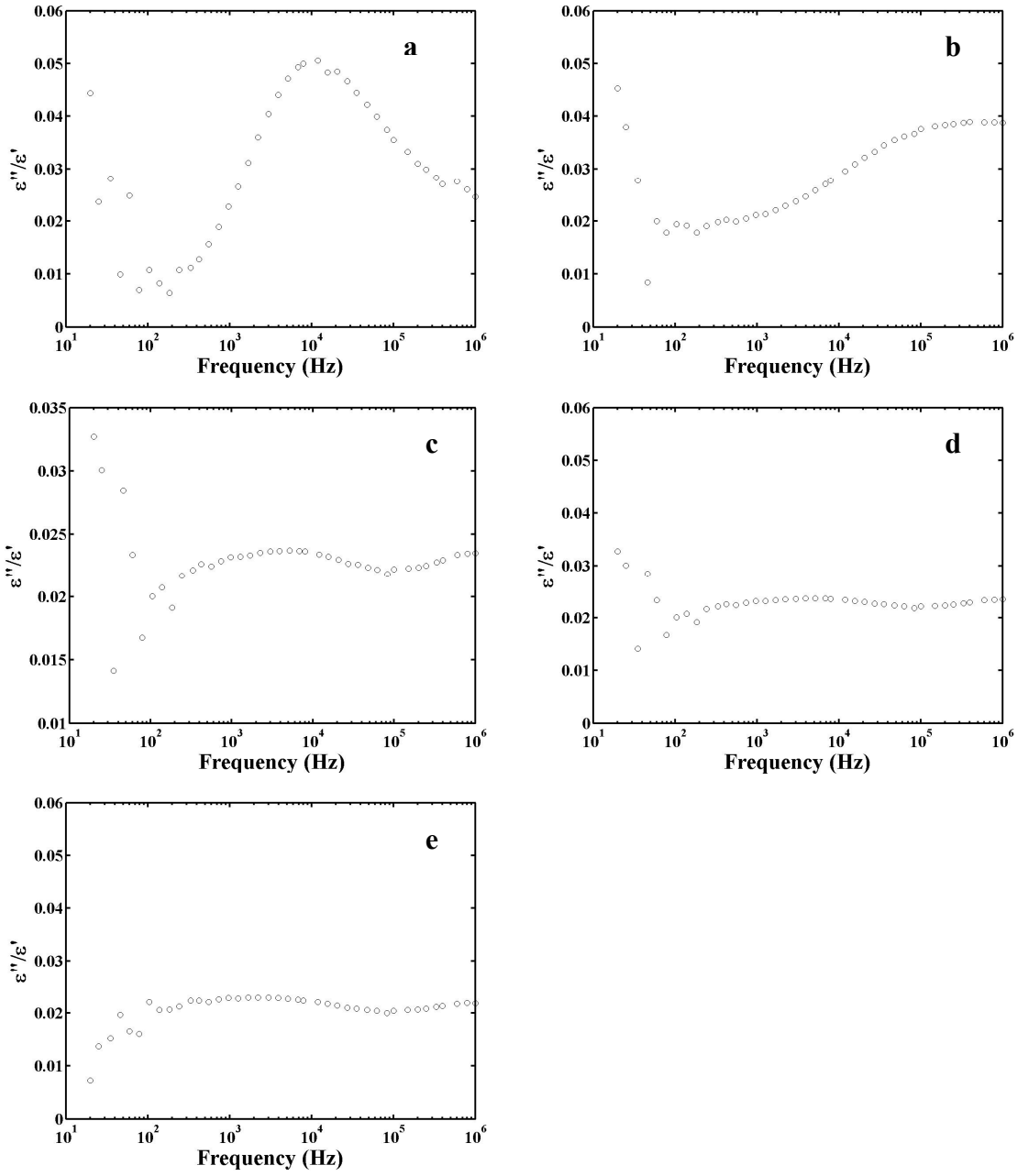

Figure 22: Dissipation factor, ε''/ε' vs. frequency of PET/CNT nanocomposite during isothermal crystallization at 120°C for 0 (a), 10 (b), 15 (c), 20 (d), and 30 (e) minutes

Discussion

The real-time dielectric data during crystallization shows a slower rate of crystallization than appears in the real-time WAXS and SAXS data. With PET, a drop in the relaxation peak intensity indicating crystallization can not be seen in the dielectric data until the sample has been held at 110°C for 17 minutes. After 30 minutes, the shift in the location of the peak indicates that crystallization is still in progress. However, in the WAXS data for PET, scattering peaks are visible after 10 minutes at 110°C and crystallization appears to have stopped after 15 minutes. This inconsistency may be cause by a change in the temperature of the sample due to the inclusion of the electrodes used during the dielectric measurements. The thermal conduction of the electrodes can interfere with the sample reaching the same temperature as the oven. Also, the thickness of the electrodes increases the separation of the heating plates and the sample. These factors may have decreased the temperature of the sample during crystallization with dielectric measurements, accounting for the decreased rate of crystallization.

The dielectric data of PET after crystallization at 100°C shows a decrease in the molecular mobility of the sample at a crystallization time of 15 minutes, but the WAXS pattern shows no increase in the crystallinity compared to the amorphous sample. At 30 minutes, there is a significant increase in the crystallinity, accompanied by a shift of the dielectric relaxation peak to a lower frequency. The dielectric measurement was made at 95°C. The sample may have begun to crystallize over the time the dielectric measurement was taken, approximately 5 minutes, explaining the discrepancy between the WAXS and dielectric measurements. However, at 95°C, the rate of crystallization of PET is slow, as shown by the lack of crystallization after holding for 15 minutes at 100°C. The drop in

the dielectric peak with little crystallization can best be explained with a heterogeneous model for the arrangement of lamellae. Initially, when only a small amount of crystallization has occurred, the mobility of the rigid amorphous phase between adjacent lamellae begins to be restricted, creating a decrease in the dielectric peak with little increase in crystallinity. After significant crystallization has occurred, there is spherulite impingement and secondary crystallization develops in the amorphous region between lamellar stacks, as indicated by the shift in the dielectric peak to lower frequencies.

The WAXS and SAXS data indicate that isothermal crystallization occurs at a more rapid rate in the PET/CNT nanocomposite than it does in the pure PET. This can be explained by the carbon nanotubes providing nucleation sites for the crystallization of the PET. The carbon nanotubes serving as nucleation sites increase the ability of the PET to begin crystallization.

References

1. D. Bower. *An Introduction to Polymer Physics*. Cambridge University Press (Cambridge, 2002).

2. R. Androsch, B. Wunderlich, *Polymer*, 46 (2005) 12556.

3. C. Alvarez, I. Sics, A. Nogales, Z. Denchev, S.S. Funari, T.A. Ezquerra, *Polymer*, 45 (2004) 3953.

4. B. B. Sauer and B. S. Hsiao, *Polymer*, 36 (1995) 2553.

5. S. Reich, C. Thomsen, J. Maultzsch, *Carbon Nanotubes*. Wiley-VCH (Berlin, 2004).

6. S. Iijima, *Nature*, 354 (1991) 56.

7. M. O'Connell, *Carbon Nanotubes: Properties and Applications*. CRC Press (Boca Raton, 2006).

8. A. R. Blythe, *Electrical Properties of Polymers*. Cambridge University Press (Cambridge, 1979).

9. P. Fishbane, S. Gasiorowicz, S. Thornton, *Physics for Scientists and Engineers*. Pearson Prentice Hall (Upper Saddle River, 2005).

10. F. Cser, *Journal of Applied Polymer Science*, 80 (2001) 2300.

11. L. Yu, Matlab program titled *Real-time Dielectric*, 2008.

12. P. Cebe, Matlab program titled *X27CorrectGui*, 2008.